Available at
www.ElsevierComputerScience.com
POWERED BY SCIENCE DIRECT®

PERGAMON

Pattern Recognition 37 (2004) 1519–1532

PATTERN RECOGNITION
THE JOURNAL OF THE PATTERN RECOGNITION SOCIETY

www.elsevier.com/locate/patcog

Matching of dental X-ray images for human identification☆

Anil K. Jain*, Hong Chen

Department of Computer Science & Engineering, Michigan State University, 3115 Engineering Building, East Lansing MI 48824, USA

Received 23 May 2003; received in revised form 24 October 2003; accepted 22 December 2003

Abstract

Forensic dentistry involves the identification of people based on their dental records, mainly available as radiograph images. Our goal is to automate this process using image processing and pattern recognition techniques. Given a postmortem radiograph, we search a database of antemortem radiographs in order to retrieve the closest match with respect to some salient features. In this paper, we use the contours of the teeth as the feature for matching. A semi-automatic contour extraction method is used to address the problem of fuzzy tooth contours caused by the poor image quality. The proposed method involves three stages: radiograph segmentation, pixel classification and contour matching. A probabilistic model is used to describe the distribution of object pixels in the image. Results of retrievals on a database of over 100 images are encouraging.

Keywords: Forensic dentistry; Dental radiographs; Segmentation; Matching; Human identification; Biometrics

1. Introduction

The objective of the research reported here is to automate the process of forensic dentistry. The main purpose of forensic dentistry is to identify deceased individuals, for whom other cues of biometric identification (e.g., fingerprint, face, etc. [1]) may not be available. In forensic dentistry, the postmortem (PM) dental record is compared against antemortem (AM) records pertaining to some presumed identity. A manual comparison between the AM and PM records is based on a systematic dental chart prepared by forensic experts [2,3]. In this chart, a number of distinctive features are noted for each individual tooth. These features include properties of the teeth (e.g., tooth present/not present, crown and root morphology, pathology and dental restorations), periodontal tissue features, and anatomical features. Depending on the number of matches, the forensic expert rejects or confirms the tentative identity. There are several advantages for automating this procedure. First, an automatic process will be able to compare the PM records against AM records pertaining to multiple identities in order to determine the closest match. Second, while a manual (non-automated) system is useful for *verification* on a small data set, an automatic (or semi-automatic) system can perform *identification* on a large database.

For the automated identification, the dental records are usually available as radiographs (Fig. 1). An automated dental identification system consists of two main stages: feature extraction and feature matching [4]. During feature extraction, certain salient information of the teeth such as contour, artificial prosthesis, number of cuspids, etc. is extracted from the radiographs. In this paper, the feature extracted is the tooth contours because they remain more invariant over time compared to some other features of the teeth. A logical diagram of the proposed dental identification system is shown in Fig. 2. The feature extraction stage consists of the radiograph segmentation and the contour extraction. In an earlier paper [4], the authors presented a contour extraction method based on edge detection. However, due to substantial noise that is usually present in radiograph images, the edge-detection-based method does not perform consistently across all the images in our database. Also, the manual selection of the region of interest (ROI) in Ref. [4] is time

☆ This research was supported by the National Science Foundation Grant EIA-0131079.

* Corresponding author. Tel.: +1-517-355-9282, fax: +1-517-432-1061.

E-mail addresses: jain@cse.msu.edu (A.K. Jain), chenhon2@cse.msu.edu (H. Chen).

0031-3203/$30.00 © 2003 Pattern Recognition Society. Published by Elsevier Ltd. All rights reserved.
doi:10.1016/j.patcog.2003.12.016

(a)

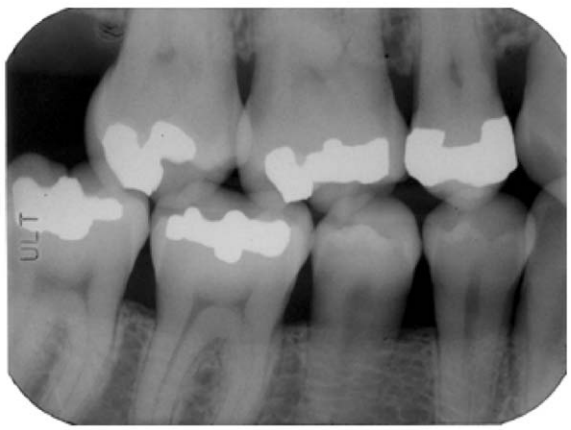

(b)

Fig. 1. Postmortem (PM) (a) and antemortem (AM) (b) dental radiographs of the same person.

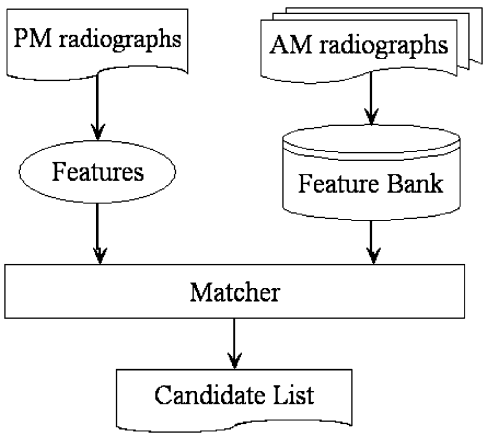

Fig. 2. The logical diagram of the dental biometrics system.

consuming and is counter to our goal of automated identification. In this paper, we have developed a segmentation algorithm for the detection of ROI. Further, a probabilistic

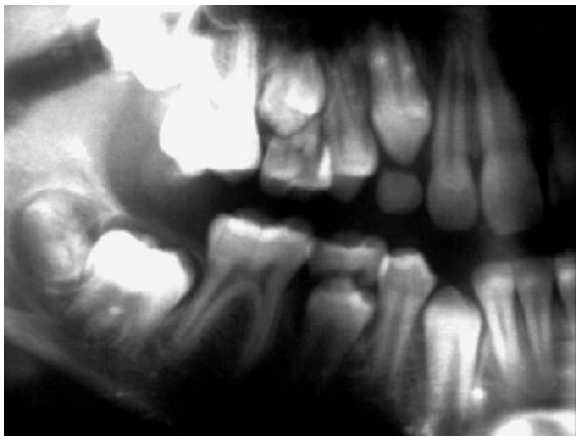

Fig. 3. A radiograph with abnormal teeth appearance and poor image quality.

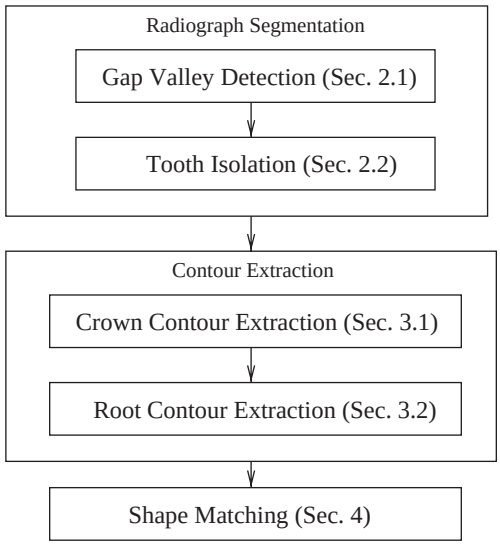

Fig. 4. The diagram of the processing flow.

method is introduced to automatically find the contours of teeth. However, a fully automatic feature extraction method is still not capable of handling the large variance in image quality and the appearance of teeth (see Fig. 3). Thus, human intervention is needed to initialize certain algorithmic parameters and correct errors in some problematic images. In the feature matching stage, the extracted contours from the PM radiograph (query image) are compared against those extracted from AM records that are stored in a database. A matching score is computed to measure the similarity between the two given radiographs. A candidate list of potential matches is then generated for human experts to make further decisions.

A diagram of the processing flow is shown in Fig. 4. In the following sections, we will provide the detail of the

radiograph segmentation (Section 2), contour extraction (Section 3) and matching (Section 4) stages of this proposed dental identification system. Experimental results on a small dental radiograph image database are also presented.

2. Radiograph segmentation

The goal of radiograph segmentation is to segment the radiograph into blocks such that each block has a tooth in it. This helps us define the ROI associated with every tooth. For simplicity, we assume there is one row each of maxillary (upper jaw) and mandibular (lower jaw) teeth in the image—this assumption is generally true except in the case of small children who are at the age of teeth formation (see Fig. 5). After the rows of upper and lower teeth are separated, each tooth needs to be isolated from its neighbors.

2.1. Gap valley detection

Let us first consider a simple case (see Fig. 6). We sum the intensities of pixels along each row parallel to the x-axis. Since the teeth usually have a higher gray level intensity than the jaws and other tissues in the radiographs due to their higher tissue density, the gap between the upper and lower teeth will form a valley in the y-axis projection histogram, which we call the *gap valley*. However, there could be many valleys in the projection, and in appearance, the gap valley is not different from other valleys. To detect the gap valley, a user-assisted initialization is needed. The procedure for detecting the gap valley is as follows:

Suppose the user initializes the estimated position, $\hat{y}$, of the gap between the upper and lower jaws. Let $v_i, i = 1, 2, \ldots, m$ be the valleys detected in the projection histogram with D_i being the depth of v_i, and y_i being the position of

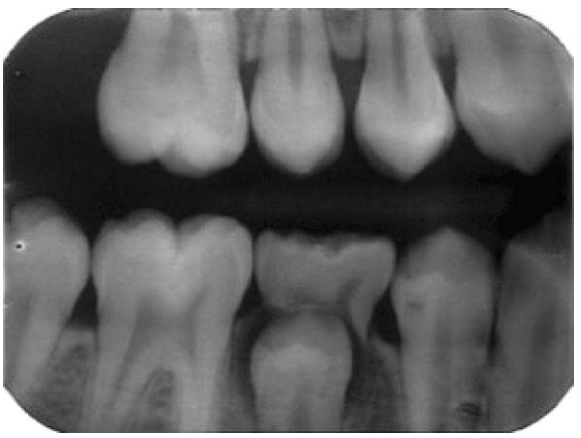

Fig. 5. The dental radiograph of a child at the age of teeth formation. A new adult tooth is under the first molar in the lower jaw, so the assumption of one row each of maxillary and mandibular teeth is not satisfied.

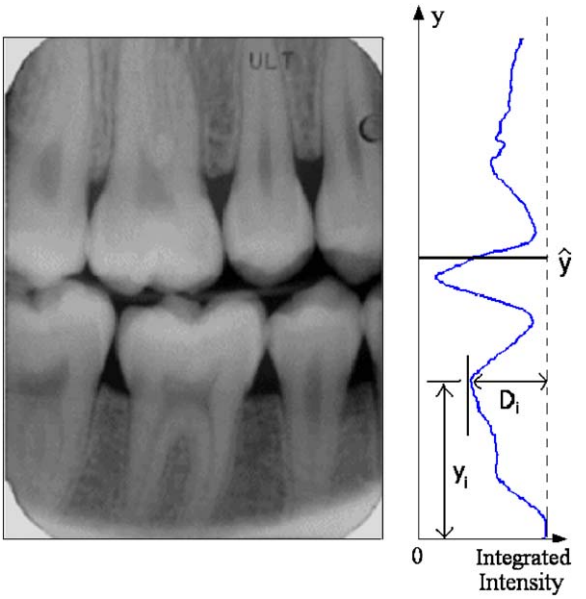

Fig. 6. Integral projection on the y-axis.

v_i (Fig. 6). Among these valleys, only one of them is the gap valley. Let $p_{v_i}(D_i, y_i)$ be the probability that v_i (with attributes D_i and y_i) is the gap valley. Then, assuming the independence between D_i and y_i, this probability is computed as

$$p_{v_i}(D_i, y_i) = p_{v_i}(D_i)\, p_{v_i}(y_i), \tag{1}$$

where

$$p_{v_i}(D_i) = c\left(1 - \frac{D_i}{\max_k D_k}\right), \tag{2}$$

$$p_{v_i}(y_i) = \frac{1}{\sqrt{2\pi}\sigma} \mathrm{e}^{-(y_i - \hat{y})^2/\sigma^2}. \tag{3}$$

In the above expression (2), the factor c is a normalizing constant to ensure $p_{v_i}(D_i)$ satisfies that a probability mass function sums up to 1, and $p_{v_i}(D_i)$ is the likelihood of the gap valley having the pixel intensity of D_i. It is based on the fact that lower the intensity, the larger the likelihood that it is the gap valley. The area of the gap valley in the image corresponds to the soft tissue in the mouth, while other areas corresponds to the jaw bones. The pixels of bones usually have higher intensities than the pixels of the soft tissue, so it is reasonable to assume the pixel intensity of the gap valley is lower than other valleys. In Eq. (3), $p_{v_i}(y_i)$ describes the likelihood of the gap valley to be at y_i. It is the normal distribution of the distance between the true position and the estimated position of the gap valley. The term σ accounts for the fact that the user initialization has some errors due to fatigue or carelessness. We assume the distribution of the error is a Gaussian, because the larger the error, the lower the probability for its occurrence. After an estimate $\hat{y}$ is given,

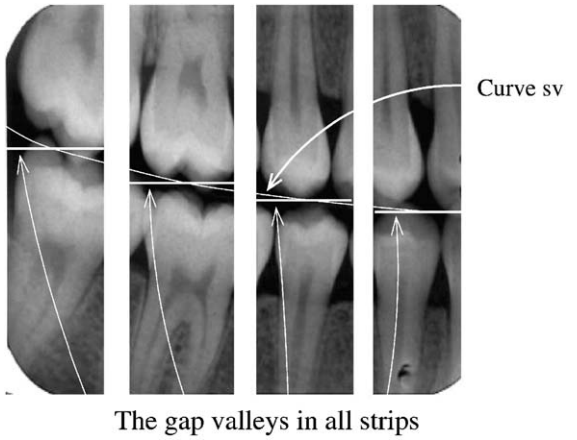

Fig. 7. Use of a spline function to connect the gap valleys in all strips into a smooth curve.

if v_i is the gap valley, then the likelihood for it to be at y_i is $p_{v_i}(y_i)$. Let v^* be the gap valley defined previously, then

$$p_{v^*}(D^*, y^*) = \max_i p_{v_i}(D_i, y_i). \quad (4)$$

For those images where the gap between the jaws is not exactly parallel to the x-axis, we divide the image into vertical strips, and apply the above method individually on each strip. If the user-provided estimate $\hat{y}$ is for a strip s, then after the position of the gap valley y_s^* in this strip is detected, for the neighboring strip s', $\hat{y}_{s'}$ is automatically updated as $\hat{y}_{s'} = y_s^*$. In some images, the inhomogeneous X-ray intensities cause the intensity of teeth pixels to change smoothly, yet significantly, over the whole image. The above step of partitioning the image into strips also addresses this problem. After the positions of $y_i^*, i = 1, 2, \ldots, m$ are detected in each strip, a spline function [5] is used to form a smooth curve sv, which separates the upper and lower teeth (Fig. 7).

2.2. Tooth isolation

The method to isolate each tooth from its neighbors is similar to the method to separate the lower and upper jaws. From the lower/upper segmentation, we determine a curve sv that defines the boundary of each row of the teeth (see Fig. 8). For the upper teeth, we sum the intensity of pixels in each line perpendicular to the valley sv (Fig. 8). The gaps between the neighboring teeth cause the valleys in the projection as shown in Fig. 8. By locating these gaps, the neighboring teeth can be segmented. A similar procedure is then used to segment the lower teeth also. A few segmentation results are shown in Fig. 9. Due to the poor quality of some images, segmentation errors are unavoidable. The errors are categorized into over-segmentation and under-segmentation. The user can delete the segmentation lines of over-segmentation and add lines for under-segmentation.

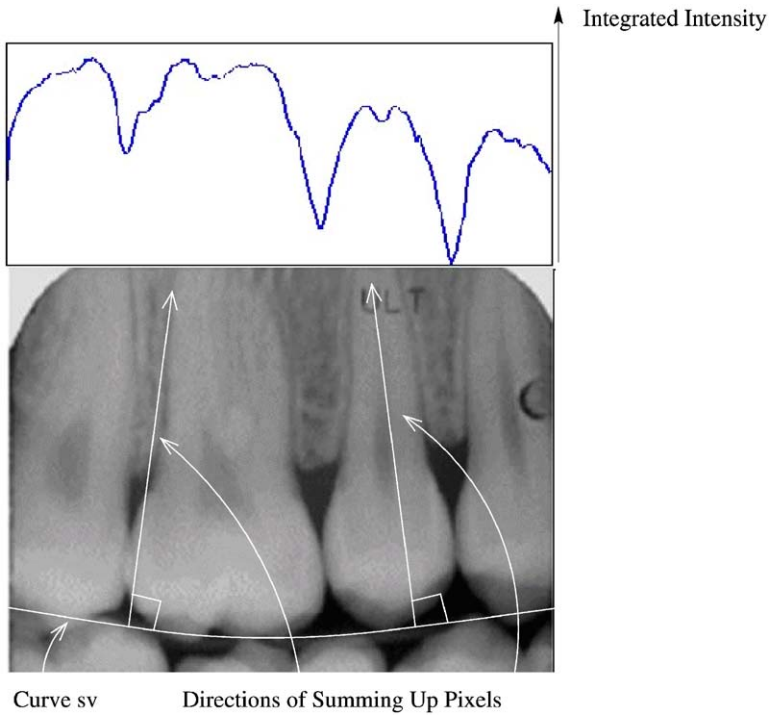

Fig. 8. Integral projection of pixels of the upper teeth along the lines perpendicular to the curve of the valley.

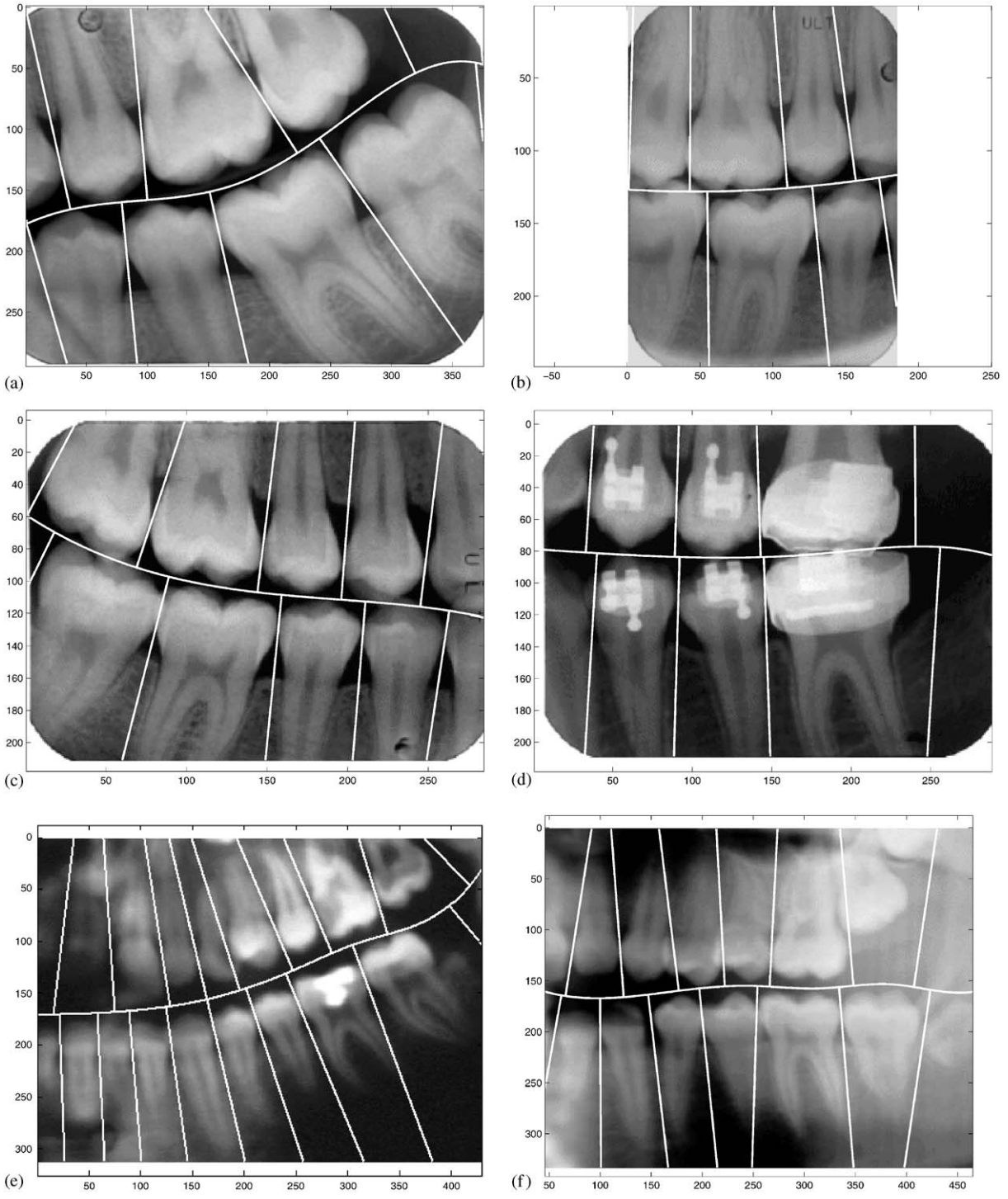

Fig. 9. Segmentation results of radiographs by integral projection.

Based on the segmentation output, an enclosing rectangle that tightly fits the segmented area, called the ROI, is constructed for each tooth. A point inside this rectangle, which will be used in shape extraction, is chosen and called the Crown Center, C. The distance of C to the top of the rectangle is one third the length of the ROI,

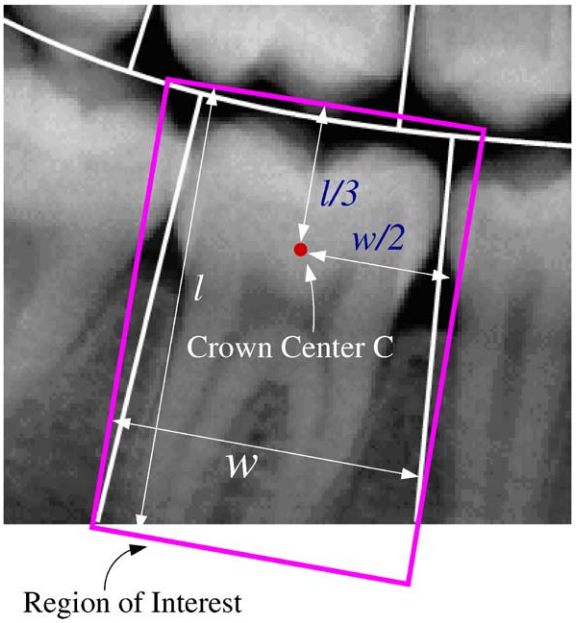

Fig. 10. The generation of ROI and the crown center.

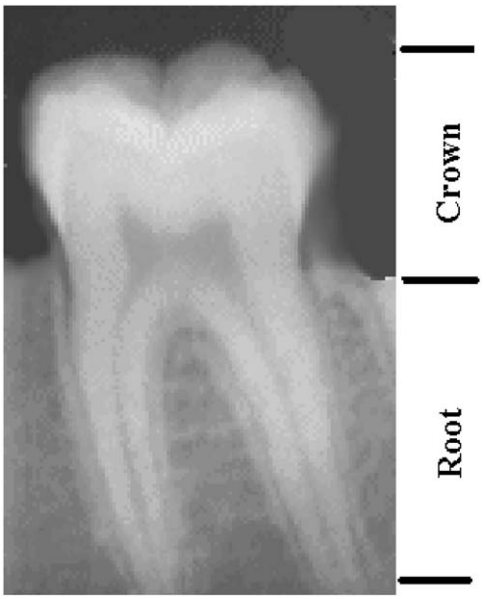

Fig. 11. Two parts of a tooth: crown and root.

and the distance of C to the other two sides are equal (Fig. 10).

3. Contour extraction

A tooth has two main parts: the *crown*, which is above the gumline, and the *root*, which sits in the bone below the gum (Fig. 11). Due to the overlap of the tooth root image with the image of the jaws, the root is not as visible as the crown in the radiographs due to the lower differential in tissue density [6,7]. Thus the crown is identified first, followed by the root contour extraction.

3.1. Crown shape extraction

By drawing a line through the crown center, the ROI is divided vertically into two rectangles: the crown area and the root area. The crown area has two classes of pixels: the tooth pixels ω_t and the background pixels ω_b. Suppose the pixel intensity is denoted as I, we can estimate the probability density function $p(I)$ either using the Parzen window approach with a Gaussian kernel [8] or using a mixture of two components. Taking the mixture approach, we write the density function as

$$p(I) = p(I|\omega_b)P(\omega_b) + p(I|\omega_t)P(\omega_t), \tag{5}$$

where $p(I|\omega_b)$ is the distribution of intensities of background pixels and $p(I|\omega_t)$ is the distribution of intensities of teeth pixels. The background pixels represent the soft tissue in the mouth and have lower intensities, so it is assumed that $p(I|\omega_b)P(\omega_b)$ is the first Gaussian component in $p(I)$, as shown in Fig. 12. By approximating the first mode of $p(I)$, we can identify $p(I|\omega_b)P(\omega_b)$. We do not need to care what is the distribution of the other component.

According to the Bayes rule, the posteriori probability of a pixel with intensity I being a background pixel given intensity I is

$$p(\omega_b|I) = \frac{p(I|\omega_b)P(\omega_b)}{p(I)}. \tag{6}$$

Since $p(I|\omega_b)P(\omega_b)$ and $p(I)$ have been identified, $p(\omega_b|I)$ can be resolved.

As this is a two-class problem, $p(\omega_t|I)$ is computed as

$$p(\omega_t|I) = 1 - p(\omega_b|I). \tag{7}$$

To detect the contour of the tooth crown, we perform a radial scan from the crown center C (Fig. 13(a)). Specifically, we draw a radial line from the crown center C. For each point P on the line, let P_{inner} and P_{outer} be the neighbors of P along the radial line. Then the probability for the point P to be a point on the contour of the current tooth (classified as E) is defined as

$$p(E) = p(\omega_b|I_{outer}) \cdot p(\omega_t|I_{inner}), \tag{8}$$

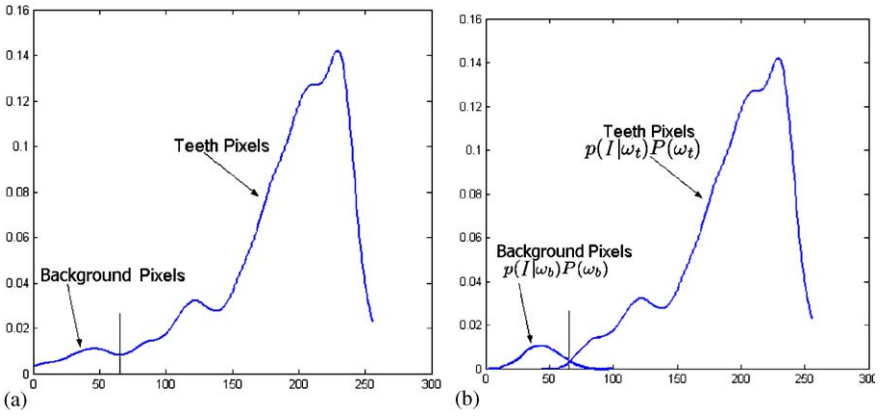

Fig. 12. Probability density functions of (a) $p(I)$ and (b) $p(I|\omega_b)P(\omega_b)$ and $p(I|\omega_t)P(\omega_t)$. $p(I|\omega_b)P(\omega_b)$ is a Gaussian component.

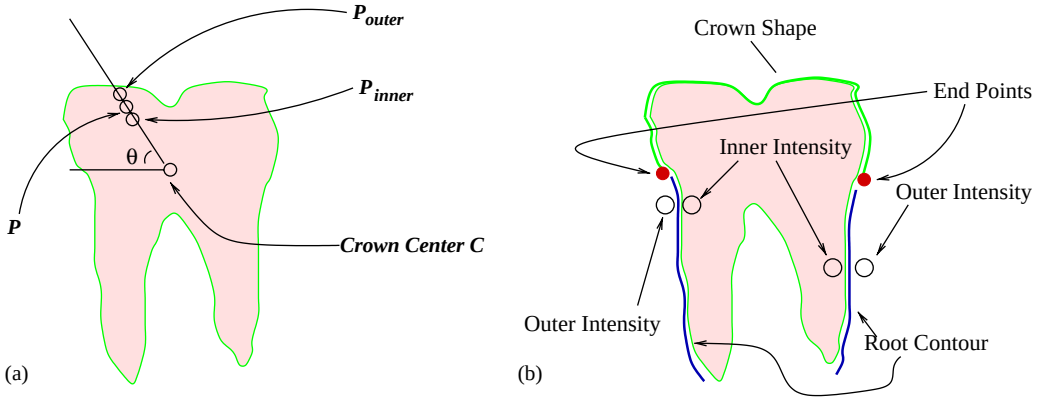

Fig. 13. Inner intensity and outer intensity.

where I_{inner} and I_{outer} are the intensities of points P_{inner} and P_{outer}. The point with the maximum probability $p(E)$ along this radial line is labelled as a contour point. The angle of the radial line, θ, is varied in the range $0 \leqslant \theta \leqslant \pi$ (Fig. 13(a)), and a contour point is identified for each angle. These contour points are connected to form the crown shape (Fig. 13(b)).

3.2. Root shape extraction

Once the crown shape is extracted, we traverse from the two ends of the shape boundary to find the root boundary. The left end of the crown is set as the first point on the left contour of the root, and the right end of the crown is the first point of the right contour. We determine the position of each new contour point on the root boundary by the position of the previous contour point and its own *context*. As a measurement of the *context*, we define two attributes at each point: I_{inner} for the *inner intensity* of the contour and I_{outer} for the *outer intensity*. For the left contour, *inner intensity* is the average intensity of a small region to the right of the contour, and *outer intensity* is the average intensity of a small region to the left of the contour; for the right contour, it is just the opposite (see Fig. 13(b)). Our aim is to find the root contour that maximizes the difference between I_{inner} and I_{outer}. In other words, for the teeth in the lower jaws, if the ith point on the left/right root contour has coordinates (x_i, y_i), the $(i+1)$th point, (x_{i+1}, y_{i+1}), is computed iteratively as

$$x_{i+1} = \arg \max_{x_i - r \leqslant x \leqslant x_i + r} (I_{inner} - I_{outer}),$$

$$y_{i+1} = y_i + h, \tag{9}$$

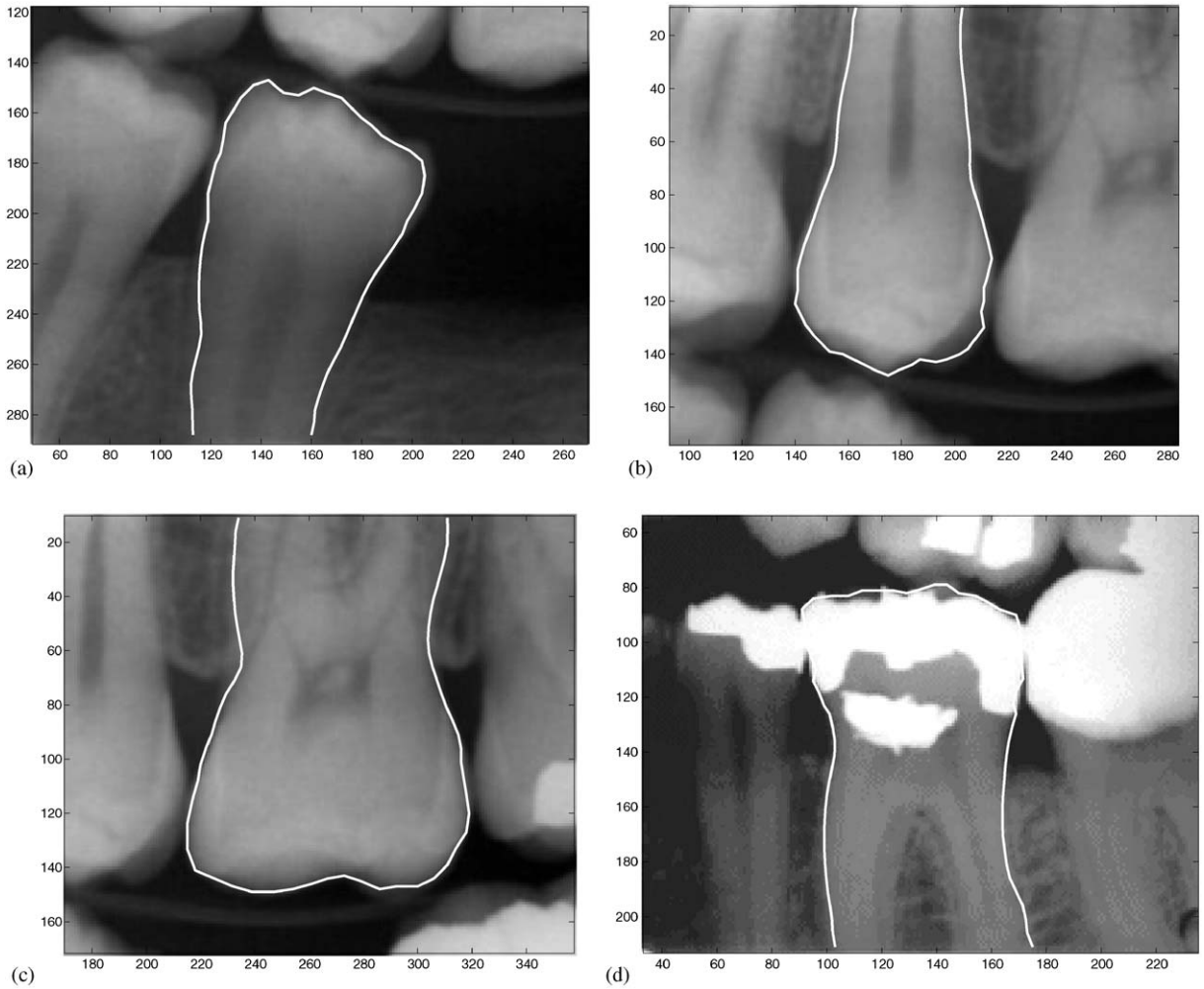

Fig. 14. Some examples of extracted tooth shapes.

where r is the radius of the search space and h is the increment in the vertical position for each new point. The iteration ends when y_i increases beyond the image boundary, or $\max_{x_i-r\leqslant x\leqslant x_i+r}(I_{inner} - I_{outer})$ is less than a threshold. Fig. 14 shows some examples of extracted tooth shapes.

Once we get the crown contour and the root contour, we connect them to form the contour of the whole tooth. In the next section, we will match these contours for identification.

4. Shape matching

The contours extracted from the query image must be matched to the contours extracted from the database images. Because the PM images are usually captured several years after the AM images are acquired, the shapes of the teeth could have changed due to teeth extraction or the growth of teeth. If we assume there are no such changes, the AM and PM radiographs differ only in terms of scaling, rotation, translation and the change of the imaging angle. Because of the criteria of the intraoral radiographic examinations [6], the change of imaging angle is not severe. So, currently, we omit this variation. Other differences can be factored out by a *rigid transformation* [9]. As the optimization criteria for the transformation, we first define the matching distance (MD) between pairs of radiographs.

4.1. Matching distance

Given a query image **Q**, we generate several sub-images from every database image, each sub-image containing the

Fig. 15. Some images in the database of AM radiographs.

same number of teeth as the query image. If the teeth in query image $\mathbf{Q}$ and database sub-images $\mathbf{D}$ are labelled as $1, 2, \ldots, N$ from left to right, then $\mathbf{Q} = \{\Gamma_i\}_{i=1}^{N}$ and $\mathbf{D} = \{\Phi_i\}_{i=1}^{N}$. For the convenience of notation, let Γ_i and Φ_i refer to the points in the contour of the tooth also, then $\Gamma_i = \{\gamma_{i,j}\}_{j=1}^{N_{\Gamma_i}}$ and $\Phi_i = \{\phi_{i,j}\}_{j=1}^{N_{\Phi_i}}$.

Given a transformation T, a query image $\mathbf{Q}$ and a database subimage $\mathbf{D}$, we define the *matching distance* MD that needs to be minimized. Specifically, $MD(T, \mathbf{Q}, \mathbf{D})$ is the summation of $D(T, \Gamma_i, \Phi_i)$ over all the N pairs, defined by

$$MD(T, \mathbf{Q}, \mathbf{D}) = \sum_{i=1}^{N} D(T, \Gamma_i, \Phi_i), \tag{10}$$

where

$$D(T, \Gamma_i, \Phi_i) = \sum_{\phi_{i,j} \in \Phi_i} \min_{\gamma \in \Gamma_i} \|T(\phi_{i,j}) - \gamma\|. \tag{11}$$

Note that $D(T, \Gamma_i, \Phi_i)$ is the distance between a pair of teeth, Γ_i and Φ_i.

4.2. Contour alignment

Determining the best contour alignment requires us to find the rigid transformation T, which minimizes the MD defined above. The rigid transformation, T, is a function of the form

$$T : R^2 \to R^2, \quad T(\phi) = A\phi + \tau, \tag{12}$$

where $\phi = (x, y)^t$ represents a point in the query shape, $T(\phi)$ is the result of applying the transformation T on ϕ, A is the transformation matrix, and τ is a translation vector. The parameters A and τ can be represented as

$$A = \begin{pmatrix} \cos\theta & \sin\theta \\ -\sin\theta & \cos\theta \end{pmatrix} \begin{pmatrix} \mathscr{S}_x & 0 \\ 0 & \mathscr{S}_y \end{pmatrix},$$

$$\tau = \begin{pmatrix} \tau_x \\ \tau_y \end{pmatrix}. \tag{13}$$

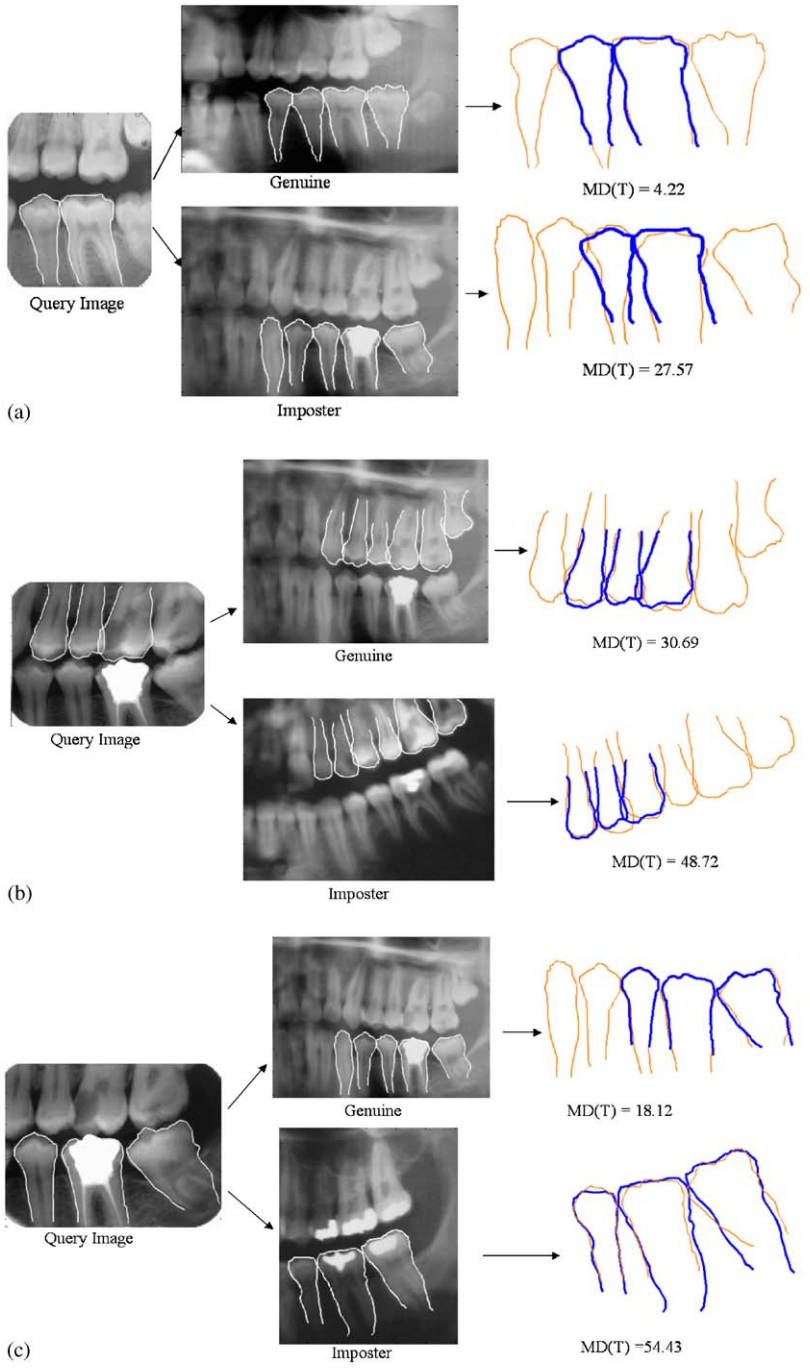

Fig. 16. Examples of matching. The gray lines represent the teeth shapes in the AM images; the black lines represent the query shapes after the transformation T. Note that in these examples, the matching distance for the genuine AM images is smaller than the matching distance for the imposter AM images.

There are a total of 5 parameters in the transformation T, $\{\theta, \mathscr{S}_x, \mathscr{S}_y, \tau_x, \tau_y\}$, where θ is the rotation angle, $\mathscr{S}_x$ and $\mathscr{S}_y$ are the horizontal and vertical scale factors, and τ_x and τ_y are horizontal and vertical translations. These parameters are optimized by searching for the best alignment between the transformed query shape and the database shape.

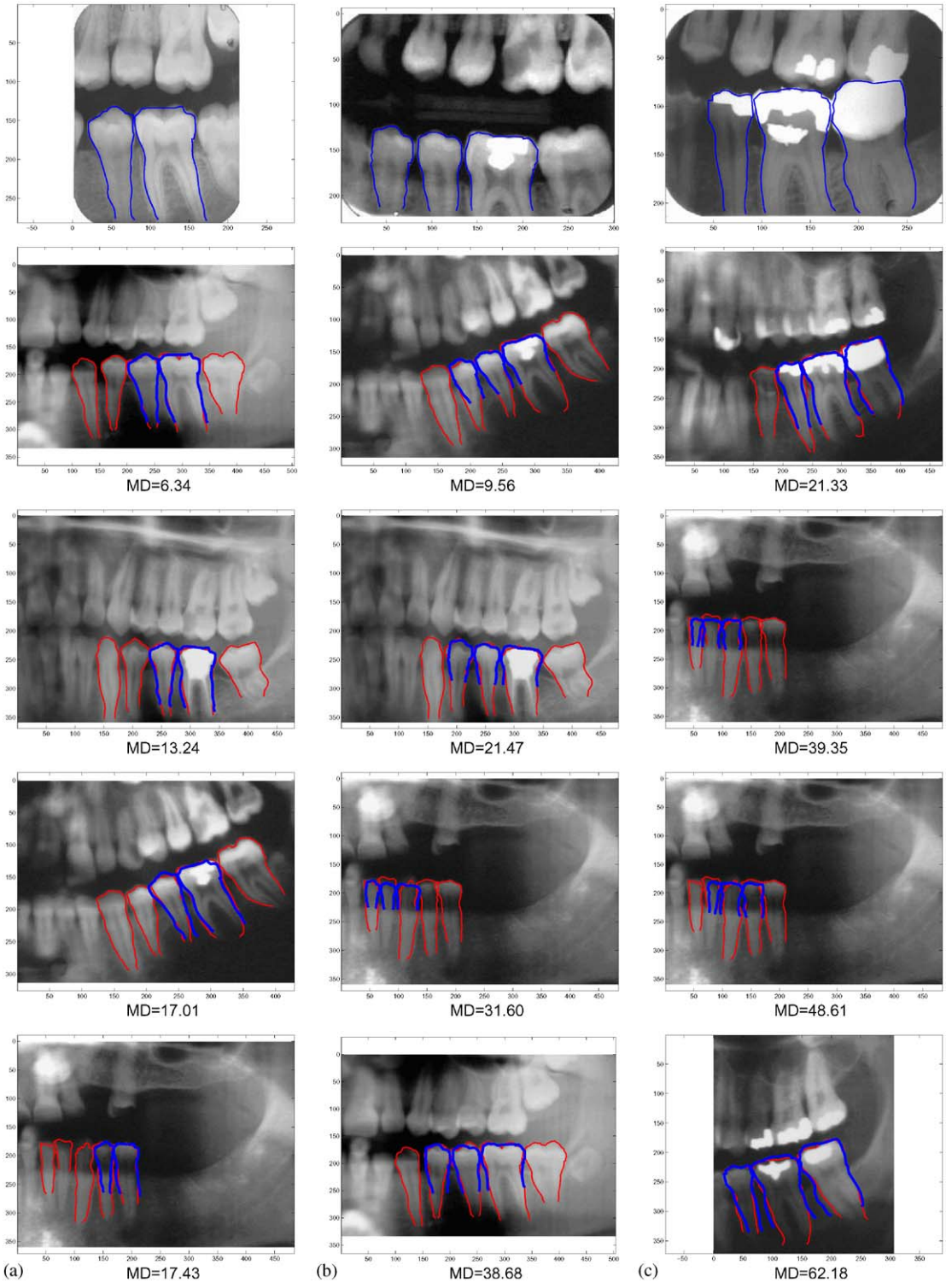

Fig. 17. The top 4 retrievals for 3 different queries. The first image in each column is the query image and the remaining four images in each column are the top 4 retrievals. The genuine AM images are ranked first for these three queries. Matching distance is shown with each retrieval.

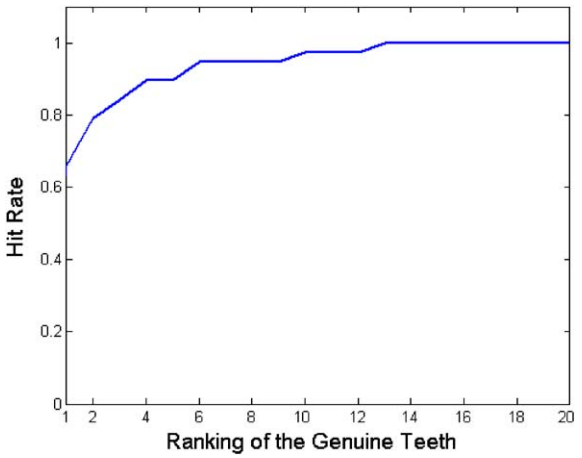

Fig. 18. Retrieval performance.

By finding the *tightest fitting rectangle* for the groups of query shapes and database shapes, the parameters in the transformation T are initialized as

$$\theta = \theta_d - \theta_q,\ \mathscr{S}_x = W_d/W_q, \quad \mathscr{S}_y = \mathscr{S}_x,$$
$$\tau_x = Cd_x - Cq_x,\ \tau_y = Cd_y - Cq_y, \tag{14}$$

where θ_q and θ_d are the orientations of the tightest fitting rectangles for the query shapes and the database shapes, respectively, W_q and W_d are the widths of the rectangles, and (Cq_x, Cq_y) and (Cd_x, Cd_y) are the centers of the rectangles.

A sequential quadratic programming (SQP) method [10–13] is applied for the optimization of the parameters of T. Ranges of the parameter values are set to properly guide the optimization procedure. Finally, a ranking of the database images is generated with respect to their minimized $MD(T, \boldsymbol{Q}, \boldsymbol{D})$ value in ascending order, because a smaller distance indicates a better match.

5. Experiments

The proposed dental X-ray-based identification method has been applied to 38 query images for retrieval from a database, which contains 130 AM images. Fig. 15 shows some of the AM images in the database. In each query image, we divide the teeth into two groups: the teeth in the upper jaw and the teeth in the lower jaw. The teeth in the same group will not change their relative positions, while teeth from different groups will probably change their relative positions because of the opening and closing of the mouth during image capture. Therefore, we match the two groups of teeth separately.

Fig. 16 shows some examples of query images matched with a genuine and an impostor image in the database. The matching distance between the query image and the genuine teeth is smaller than that compared to the imposter teeth. Fig. 17 shows top 4 retrievals for three different query images and how the query shapes are matched to the database shapes. In our experiments, among the 38 queries, 25 genuine AM images were ranked first. For the remaining 13 queries, 5 of them were among the top 2 retrieved images and 9 were among the top 5 retrieved images. The retrieval performance curve is shown in Fig. 18. We examined the 13 query images that were not correctly matched and identified the following reasons for these mismatches: (i) poor quality of images, resulting in errors in tooth extraction, (ii) some tooth were only partially visible and (iii) the inherent similarity between teeth shapes of different individuals.

6. Conclusions and future work

A new semi-automatic method of human identification based on dental radiographs is proposed. This method involves three stages: radiograph segmentation, tooth feature extraction, and tooth feature matching. The feature utilized here is the contours of the teeth. A probabilistic model is used to describe the distribution of tooth pixels and background pixels in the image. After the tooth contours are extracted, a transformation is used to align the contours to correct the imaging geometric variations, and a matching distance is generated. The final decision is obtained with respect to the matching distances. Preliminary experiments on a small database indicate that this is a feasible approach.

However, it is difficult to apply the proposed method in situations where (i) the images are very blurred (Fig. 19(a)), (ii) the query shape is partially occluded so that there is not enough information available to characterize the teeth (e.g., upper teeth in Fig. 19(b)), (iii) there is a substantial change in the imaging angle between the AM and PM images that causes changes in the shapes of the teeth (Fig. 19(c)), and (iv) some teeth have been extracted. Some of these problems can be addressed by utilizing additional information such as artificial prothesis of the teeth, the striae patterns [7] and trabecular patterns [14].

Future work will involve utilizing these additional sources of information to improve the reliability of person identification with dental images. Meanwhile, since several PM images are usually available for a single person and each PM image generates a list of retrievals, we are currently working on combining these results to provide a better retrieval. In addition, we are developing an image restoration algorithm to handle poor quality radiographs. We also plan to evaluate our algorithm on a larger database of dental radiographs.

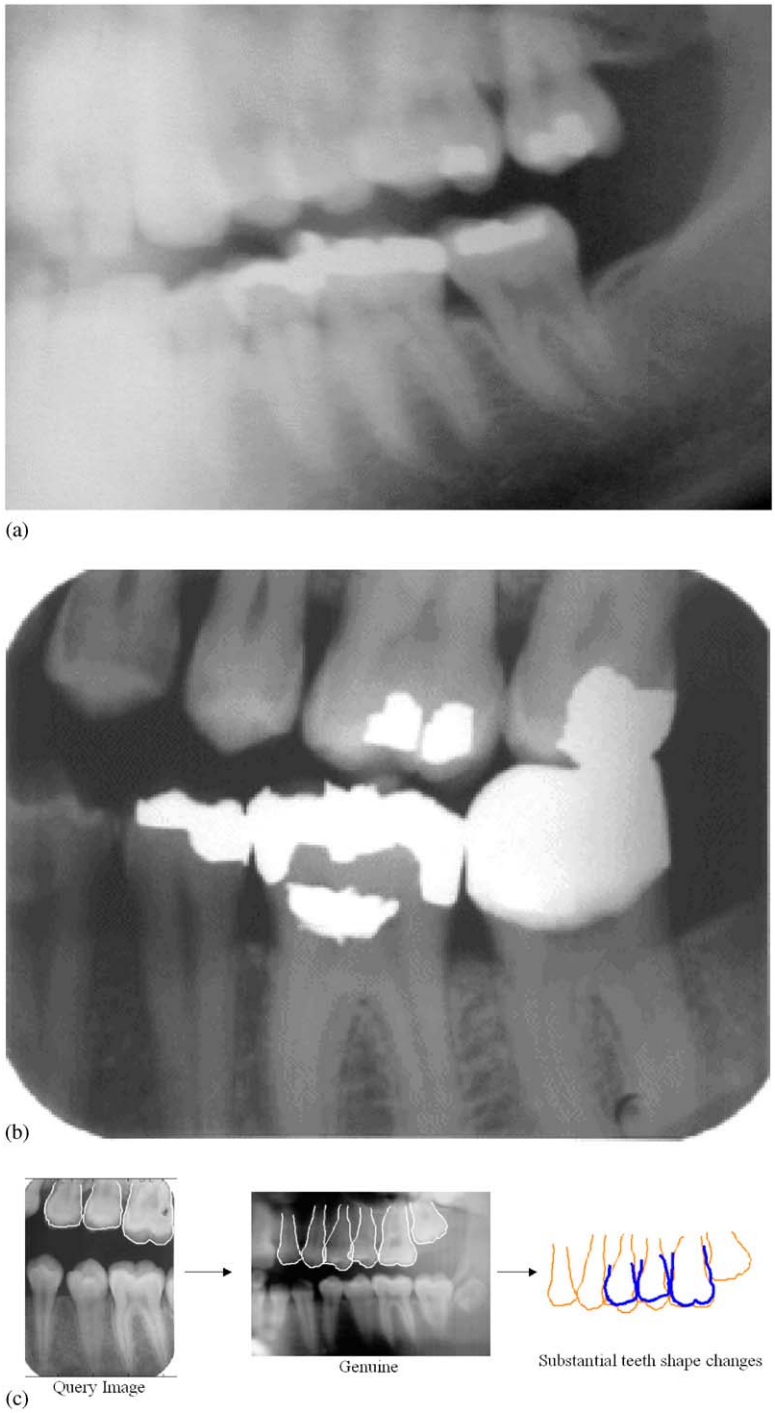

Fig. 19. Examples of query images where the proposed matching approach fails: (a) The image is too blurred for reliable shape extraction; (b) the upper teeth are only partially visible and (c) The change in the imaging angle causes substantial changes in the shapes of the teeth.

References

[1] A. Jain, R. Bolle, S. Pankanti, Biometrics-Personal Identification in Networked Society, Kluwer Academic Publishers, Dordrecht, 1999.
[2] American Board of Forensic Odontology, Body identification guidelines, J. Am. Dent. Assoc. 125 (1994) 1244–1254.
[3] I.A. Pretty, D. Sweet, A look at forensic dentistry—Part 1: the role of teeth in the determination of human identity, Br. Dent. J. 190 (7) (2001) 359–366.
[4] A.K. Jain, H. Chen, S. Minut, Dental biometrics: human identification using dental radiographs, in: Proceedings of the Fourth International Conference on AVBPA, Guildford, UK, 2003, pp. 429–437.
[5] C. deBoor, B(asic)-spline basics, in: L. Piegl (Ed.), Fundamental Developments of Computer-Aided Geometric Modeling, Academic Press, New York, 1993, pp. 27–49.
[6] P.W. Goaz, S.C. White, Oral Radiology—Principles and Interpretation, The C.V. Mosby Company, St. Louis, 1982, pp. 178–245, (Chapter 11).
[7] M. Cavalcanti, A. Ruprecht, W. Johnson, S. Thomas, J. Jakobsen, S. Paulo, Oral and maxillofacial radiology, Oral Surg. Oral Med. Oral Pathol. 88 (1999) 353–357.
[8] R.O. Duda, P.E. Hart, D.G. Stork, Pattern Classification, 2nd Edition, Wiley Interscience, New York, 2001, pp. 164–174, (Chapter 10).
[9] L.G. Brown, A survey of image registration techniques, ACM Comput. Surveys 24 (4) (1992) 325–375.
[10] T.F. Coleman, Y. Li, On the convergence of reflective Newton methods for large-scale nonlinear minimization subject to bounds, Math. Programming 67 (2) (1994) 189–224.
[11] T.F. Coleman, Y. Li, An interior, trust region approach for nonlinear minimization subject to bounds, SIAM J. Optim. 6 (1996) 418–445.
[12] P.E. Gill, W. Murray, M.H. Wright, Practical Optimization, Academic Press, New York, 1981.
[13] S.P. Han, A globally convergent method for nonlinear programming, J. Optim. Theory Appl. 22 (1977) 297.
[14] G. Jonasson, G. Bankvall, Estimation of skeletal bone mineral density by means of the trabecular pattern of the alveolar bone, its interdental thickness, and the bone mass of the mandible, Oral Surg. Oral Med. Oral Pathol. Oral Radiol. Endod. 92 (2001) 346–352.

About the Author—ANIL JAIN is a University Distinguished Professor in the Departments of Computer Science and Engineering and Electrical and Computer Engineering at Michigan State University. He was the Department Chair between 1995–1999. His research interests include statistical pattern recognition, exploratory pattern analysis, texture analysis, document image analysis and biometric authentication. Several of his papers have been reprinted in edited volumes on image processing and pattern recognition. He received the best paper awards in 1987 and 1991, and received certificates for outstanding contributions in 1976, 1979, 1992, 1997 and 1998 from the Pattern Recognition Society. He also received the 1996 IEEE Transactions on Neural Networks Outstanding Paper Award. He is a fellow of the IEEE, ACM, and International Association of Pattern Recognition (IAPR). He has received a Fulbright Research Award, a Guggenheim fellowship and the Alexander von Humboldt Research Award. He delivered the 2002 Pierre Devijver lecture sponsored by the International Association of Pattern Recognition (IAPR). He holds six patents in the area of fingerprint matching. He is the author of the following books: Handbook of Fingerprint Recognition, Springer 2003, BIOMETRICS: Personal Identification in Networked Society, Kluwer 1999, 3D Object Recognition Systems, Elsevier 1993, Markov Random Fields: Theory and Applications, Academic Press 1993, Neural Networks and Statistical Pattern Recognition, North-Holland 1991, Analysis and Interpretation of Range Images, Springer-Verlag 1990, Algorithms For Clustering Data, Prentice-Hall 1988, and Real-Time Object Measurement and Classification, Springer-Verlag 1988.

About the Author—HONG CHEN received his B.Sc. and M.Sc. degrees in Computer Science from Fudan University, Shanghai, P.R. China. He is currently working towards his Ph.D. degree in Department of Computer Science and Engineering, Michigan State University, Lansing, MI, USA. His research interests are pattern recognition, computer vision and medical signal processing.